A Power Pack Based on Organometallic Perovskite Solar Cell and Supercapacitor

Xiaobao Xu,[⊥,†] Shaohui Li,[⊥,†] Hua Zhang,[†] Yan Shen,[†] Shaik M. Zakeeruddin,[‡] Michael Graetzel,[‡] Yi-Bing Cheng,[†,§] and Mingkui Wang*[,†]

[†]Wuhan National Laboratory for Optoelectronics, School of Optical and Electronic Information, Huazhong University of Science and Technology, Wuhan, Hubei 430074, P. R. China, [‡]Laboratoire de Photonique et Interfaces, Institut des Sciences et Ingenierie Chimique, Ecole Polytechnique Federale de Lausanne Station 6, 1015 Lausanne, Switzerland, and [§]Department of Materials Engineering, Monash University, Melbourne, Victoria 3800, Australia. [⊥]These authors contributed equally.

ABSTRACT We present an investigation on a power pack combining a $CH_3NH_3PbI_3$-based solar cell with a polypyrrole-based supercapacitor and evaluate its performance as an energy pack. The package achieved an energy storage efficiency of 10%, which is much higher than that of other systems combining a PV cell with a supercapacitor. We find a high output voltage of 1.45 V for the device under AM 1.5G illumination when the $CH_3NH_3PbI_3$-based solar cell is connected in series with a polypyrrole-based supercapacitor. This system affords continuous output of electric power by using $CH_3NH_3PbI_3$-based solar cell as an energy source mitigating transients caused by light intensity fluctuations or the diurnal cycle.

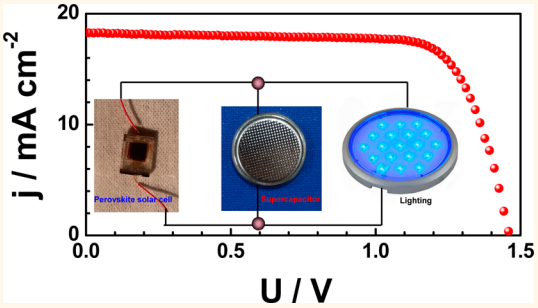

KEYWORDS: perovskite · solar cell · integrated device · supercapacitor · polarization

Organometal trihalide perovskites have shown great promise for next generation photovoltaics, due to their intriguing optoelectronic properties, such as strong absorption in the visible range,[1−3] large carrier mobility,[4,5] bipolar transport,[6,7] and a long photogenerated carrier diffusion length,[8,9] which enable realization of highly efficient photovoltaic devices. After a high power conversion efficiency (PCE) of around 15% was certified for perovskite solar cells (PSC) with mesoporous TiO_2 as a scaffold,[10] photovoltaic performance has now further increased to 17.9%.[11−14] The PCE of PSCs is expected to be able to reach 20% and then potentially beyond that of crystalline silicon solar cells through better control of the materials and processing parameters.[15] In this perspective, PSCs are one of the promising candidates for the next-generation photovoltaics with combined low cost and high efficiency. However, a caveat of PCEs is their lead content and poor stability under ambient conditions. In addition, for planar PSC configurations a slow ionic drift appears to reduce their power output under illumination hampering practical applications.[16]

Electric storage mitigating the power output swing of PV cells caused by light intensity fluctuations and the diurnal cycle is of great importance for large-scale solar conversion. Recently, attempts have been made to directly stack a photovoltaic cell and an energy storage device into one device which enables conversion and storage of solar energy.[17] The integrated energy pack provides an ideal method to store energy captured from environment, as it not only avoids energy wastage but also maintains stability of power output. For example, a combination of a solar cell with a chemical battery can work continuously regardless of the availability of sunlight.[18] These devices can also act as a buffer alleviating the problems caused by any imbalance between the solar output and energy demand. Although some devices showed promise, their overall efficiency remained low, *i.e.*, around 2%.[19−23] Note that the net efficiency considered here is lower than the PCE as it includes losses from the energy storage process. Also previous studies used a liquid electrolyte based power storage system which exhibited a lower efficiency and electrolyte leakage.[24] The electrical

* Address correspondence to mingkui.wang@mail.hust.edu.cn.

Received for review November 21, 2014 and accepted January 22, 2015.

Published online January 22, 2015
10.1021/nn506651m

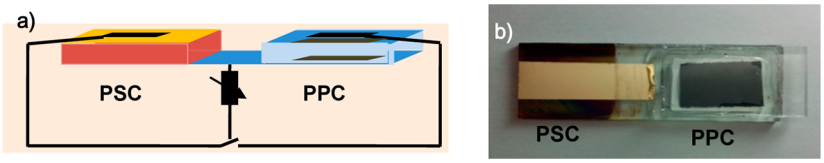

Figure 1. (a) Structural scheme of an integrated energy pack containing a $CH_3NH_3PbI_3$-based solar cell (PSC) and a ploypyrrole based supercapacitor (PPC), and (b) photograph of the integrated device.

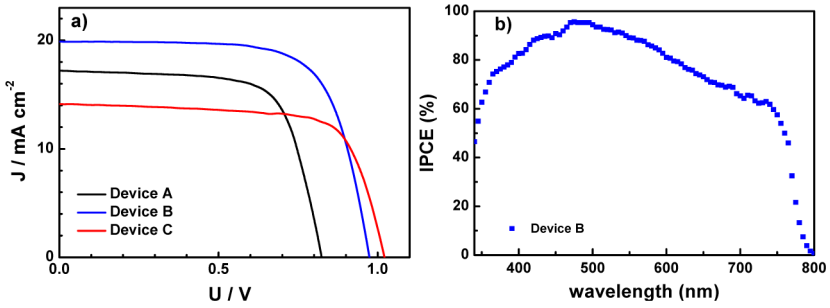

Figure 2. (a) Photocurrent density−voltage (J−V) characteristics of $CH_3NH_3PbI_3$ based perovskite solar cells with different mp-TiO_2 thickness (device A 300 nm; device B, 250 nm; device C 150 nm). (b) Photocurrent action spectra of device B using 250 nm thick mp-TiO_2. The devices were measured with mask of 0.16 cm^2.

energy of a solar cell can be storage with the aid of a supercapacitor. In this case, the supercapacitor provides both temporary energy storage and power delivery. Capacitors are suitable for storing energy. They can also be sued to compensate fluctuations in the power supply network. The sudden power failures are compensated by the capacitor so that the voltage decreases slowly instead. This storage method is of interest for solar engineering since it can be used to compensate weather-related fluctuations.

In this paper, we report on a new system enabling improved solar power conversion and storage based on the high performance PSC and polypyrrole based supercapacitor (PPC). Transient photovoltage/photocurrent decay measurements confirmed the slow interfacial electron hole recombination and provides a means to determine electron diffusion length.[8,9,25,26] Finally, we present an integrated system connecting the PSC with the PPC. The overall energy storage efficiency of integrated power pack reached 10% for the first time.

RESULTS AND DISCUSSION

We investigated a power back containing a $CH_3NH_3PbI_3$ based solar cell and a polypyrrole based supercapacitor to store electricity. The structure and working principle of the integrated power pack were developed to realize simultaneous photoelectric conversion and energy storage with high efficiency. Figure 1 presents a schematic presentation and a photograph of the device. The function of integrated power pack enables converting solar energy to electricity to drive a load (when connected in parallel) or store it in a supercapacitor (in a series connection) by turning a switch the solar cell to the supercapacitor. The stored energy can be released in the dark or boost the solar cell to achieve a high output power when the supercapacitor works in series with the solar cell.

In this study, the inorganic−organic hybrid solar cells were fabricated in a conventional configuration of mesoporous (mp)-TiO_2/$CH_3NH_3PbI_3$/spiro-OMeTAD/Au.[27,28] The thickness of (mp)-TiO_2 film infiltrated with $CH_3NH_3PbI_3$ varied between 150 and 300 nm and that of the hole transporting material (HTM, spiro-MeOTAD) was about 120 nm. Both were deposited onto the mp-TiO_2 film by spin coating. Large $CH_3NH_3PbI_3$ islands were observed on top of the mp-TiO_2 (see Supporting Information Figure S1) forming a capping layer that enhances the light harvesting by the perovskite in the 550−800 nm region.[28]

Figure 2a presents the photocurrent−voltage curves as a function of the (mp)-TiO_2 film thickness tested under 100 mW cm^{-2} AM 1.5G simulated irradiation. The photovoltaic metrics, open circuit voltage (V_{oc}), fill factor (FF), short circuit current density (J_{sc}) and power conversion efficiency PCE of the devices are tabulated in Table 1. Device B exhibited the best performance with V_{OC} = 0.974 V, J_{sc} = 19.90 mA cm^{-2} and a FF of 0.7, yielding a PCE of 13.6%. This result is consistent with earlier reports of the effect of film thickness on device performance.[29] Even though a thicker mp-TiO_2 film increases the light absorption, the EQE, and consequently the J_{sc}, decreases due to carrier recombination losses.[30] The representative device shows small hysteresis in the current−voltage curves (Supporting Information Figure S2a). The J_{SC}, V_{OC}, and FF values obtained are 18.9 mA cm^{-2}, 0.96 V, and 0.70%, respectively, yielding a PCE of 12.6% under standard AM 1.5 condition in the forward scan. Figure 2b illustrates the incident photon to electron conversion efficiency (IPCE) of the device B. It covers a broad spectral range

that extends to the near-IR region up to 800 nm, enabling efficient solar light harvesting.[31,32]

Figure 3a presents the recombination lifetime τ as a function of extracted charge density n_t for devices B and C. At identical extracted charge density n_t, the apparent charge recombination lifetime τ is longer for device C with 150 nm thick mesoporous TiO_2 film compared with device B with 250 nm thick TiO_2 film. This result implies that a thicker TiO_2 film increases the interfacial recombination, thus reducing the device's photovoltage. To value the charge collection efficiency, the diffusion length L was estimated by the equation of $L = (D \cdot \tau)^{1/2}$, where D is the charge diffusion constant. Figure 3b displays the calculated charge diffusion length as a function of irradiation intensity. In both devices, the diffusion length is estimated to be about 320 nm. Thus, when the thickness of photoanode was further increased, the charge collection would be deficient as the main cause of reducing the photovoltaic performance.

TABLE 1. Photovoltaic Metrics of Devices (Active Area: 0.2 cm^2 Measured with a Mask of 0.16 cm^2) Using a Photoanode with Various Thicknesses under AM 1.5 G Illumination

	TiO_2 film Thickness [nm]	V_{oc} [V]	J_{sc} [mA cm^{-2}]	FF	η [%]
Device A	300	0.823	17.23	0.7	9.9
Device B	250	0.974	19.90	0.7	13.6
Device C	150	1.01	14.13	0.69	9.8

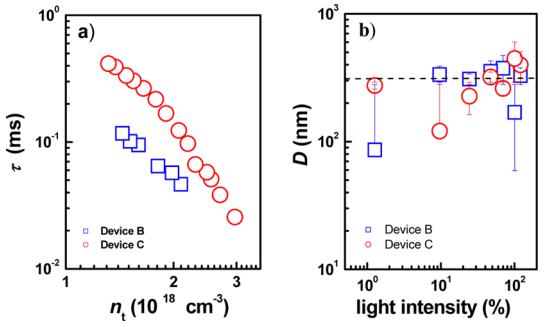

Figure 3. (a) The apparent electron lifetime (τ) as a function of the extracted charge density (n_t), and (b) the electron diffusion length (D) as a function of light intensity (% full sun intensity) obtained by transient photovoltage/photocurrent decay and charge extraction measurements.

We built a combined system affording electric power generation and storage by associating the PSC with a supercapacitor. Tests were conducted with a symmetric supercapacitor (with a size of around 1 cm^2), using two bacterial cellulose (BC) membrane/polypyrrole (PPy) nanofibers/MWCNTs films as electrodes and a cellulose acetate membrane as separator.[3] The electrochemical properties were characterized by cyclic voltammetry (CV) and galvanostatic discharging method. Figure 4a shows CV curves of symmetric supercapacitor unit with various scan rates in the range from 2 to 50 mV s^{-1}. The CV curves remained in a rectangular shape for different scan rates, indicating a high electrochemical stability and capacitance. The charge–discharge curves were nearly an ideal straight line (Figure 4b), indicating that the redox process of the active materials was carried out at a pseudoconstant rate over the whole potential window. The supercapacitor exhibited the highest A_{real} capacitance of about 572 mF cm^{-2} at a discharge current of 1 mA cm^{-2} (Figure 4c). When the current density increased from 1 to 15 mA cm^{-2}, A_{real} capacitance was retained at 82% of its original values (Figure 4c). This result reflects a high electrical conductivity as well as efficient ion transport in the porous structured film.[33,34]

In the storage mode, the PSC and supercapacitor were connected in series. When the combined device was exposed to an irradiation of standard AM 1.5G illumination, the capacitor voltage immediately increased to 0.3 V at the beginning of the charging period (see Figure 5a). Under continuous illumination the capacitor voltage slowly increased to a stable value of 0.710 V. Note that the exposed surface area to light for PSC device in Figure 5a was intentionally set at 0.06 cm^2 with a mask in order to facilitate the observation of the charging dynamics for the capacitor device. A PSC device with a big active area would significantly shorten the charging time for the capacitor. The energy (E_{PPC}) stored in the polypyrrole-based supercapacitor

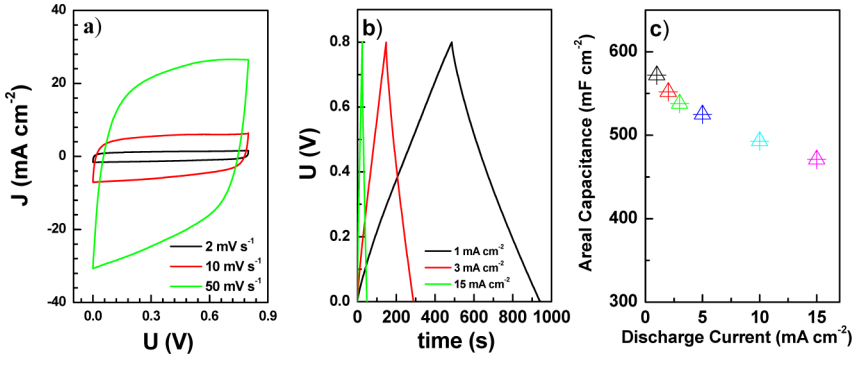

Figure 4. (a) J–V curves of the polypyrrole-based supercapacitor (PPC) under different scan rates in a two-electrode system. (b) Galvanostatic charge–discharge curves of the PPC at different charge–discharge current densities. (c) The area-specific capacitance under different discharge current density.

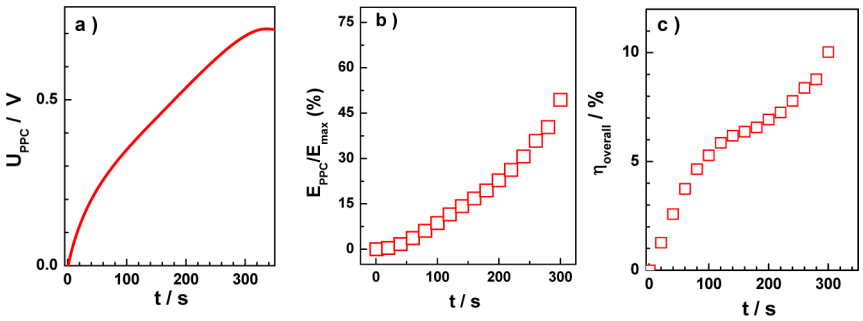

Figure 5. (a) Charging curve of a symmetric polypyrrole-based supercapacitor (PPC, area 1 cm^2) using the $CH_3NH_3PbI_3$ based solar cell operated with an illuminated area of 0.06 cm^2 as the power source; (b) the energy storage proportion (φ) of the PPC part; and (c) overall energy conversion ($\eta_{overall}$) of the stored solar energy *versus* the solar-charging time.

(C_{PPC}) during the photocharging process is calculated according to eq 1:

$$E_{PPC} = \frac{1}{2} C_{PPC} U^2 \quad (1)$$

where the value of C_{PPC} is obtained from the photocharging curve, according to eq 2.

$$C_{PPC} = \frac{dQ}{dU} = \frac{I dt}{dU} \quad (2)$$

Therefore, the energy storage proportion (φ) of polypyrrole-based supercapacitor during the charging process is defined through the following eq 3.

$$\phi = E_{PPC}/E_{max} \quad (3)$$

where E_{max} is the maximum energy that can be stored by supercapacitor. Figure 5b shows the evolution of the energy storage proportion of supercapacitor part (E_{PPC}/E_{max}) during the solar-charging process. Reaching a final value of φ near 49% needs a relative long charging time of 300 s. It is noteworthy that φ shows no significant change as the photocharging keeps going on afterward. The long charging time is caused by a mismatch of operating active areas between supercapacitor and solar cell as mentioned above. An overall conversion efficiency of the integrated device ($\eta_{overall}$) can be obtained with eq 4:

$$\eta_{overall} = E_{PPC}/(P_{in} \cdot S \cdot t_{charging}) \quad (4)$$

where P_{in} is the illuminated light density (100 mW cm^{-2}), S is the active area of solar cell, $t_{charging}$ is the charging time. Figure 5c presents the $\eta_{overall}$ during the solar-charging process. The $\eta_{overall}$ gradually increases to 10% along with the charging process. This is the highest value reported so far for an combined system comprising a solar cell and a supercapacitor.

Figure 6 presents the *J*–*V* characterization of the energy package when the supercapacitor is discharged at different voltages. The output current of the system coincides with that of the single solar cell device, while the output voltage almost equals to the sum of two individual devices. Similar to the single solar cell, the hysteresis in the integrated device is small (referring to Supporting Information Figure S2b). The detailed parameters are tabulated in Table 2. As the supercapacitor potential increases, the output voltage of the integrated device increases. It is significant that the overall output efficiency of the integrated device can reach 20% with an output voltage of 1.46 V when the voltage of PPC was set at 0.6 V. Note that both the solar cell and the capacitor contribute to total electric power output. These results demonstrate an example of a self-powered system for enlarged solar energy output density, showing great potential for

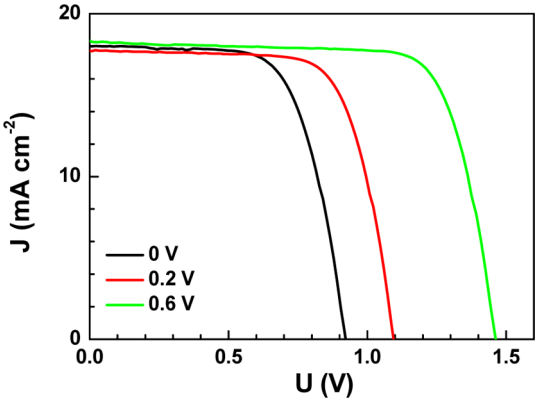

Figure 6. *J*–*V* curves of a combined system using a $CH_3NH_3PbI_3$ solar cell and a polypyrrole-based supercapacitor when the supercapacitor was charged to different potentials (0, 0.2, and 0.6 V).

TABLE 2. Photovoltaic Metrics of the Integrated Energy Package (Active Area 1 cm^2, Measured without a Mask) under AM 1.5 G Irradiation by Combining a Pervoskite Solar Cell with a Supercapacitor Discharged at Different Voltages

	parameters for the integrated device			
potential of capacitor	V_{oc} [V]	J_{sc} [mA cm^{-2}]	FF	η [%]
0 V	0.92	18.02	0.67	11.14
0.2 V	1.10	17.74	0.71	13.79
0.6 V	1.46	18.30	0.75	20.00

applications, *e.g.* in electric vehicles and mobile telephones.

CONCLUSION

We have demonstrated the first power back system based on a $CH_3NH_3PbI_3$ solar cell and a polypyrrole supercapacitor, which can be used for solar energy conversion and storage purposes. Transient photovoltage/photocurrent decay measurements revealed the carrier diffusion length to be about 320 nm for the $CH_3NH_3PbI_3$ solar cell operating under 1 sun irradiation. The overall efficiency for the conversion of solar to stored electric power was 10%, presenting the highest reported value. When a fully charged capacitor operates jointly with the $CH_3NH_3PbI_3$-based pervoskite solar cell, it can significantly boost the electrical output of the integrated device. The energy pack exhibits an open-circuit voltage of 1.45 V, contributed from both the capacitance and the solar cell at the same time.

METHODS

Solar Cell Fabrication. Zn corrosion-patterned, FTO-coated glass substrates (Tec15, Pilkington) were cleaned by ultrasonication in an alkaline, aqueous washing solution, rinsed with deionized water, ethanol and acetone, and subjected to an O_3/ultraviolet treatment for 30 min. An 80 nm-thick TiO_2 compact layer was then deposited on the substrates by aerosol spray pyrolysis at 450 °C using a commercial titanium diisopropoxide bis(acetylacetonate) solution (75% in 2-propanol, Sigma-Aldrich) diluted in ethanol (1:39, volume ratio) as a precursor and oxygen as the carrier gas. After cooling to room temperature (~25 °C), the substrates were treated in a 0.04 M aqueous solution of $TiCl_4$ for 30 min at 70 °C, rinsed with deionized water, and dried at 500 °C for 20 min. Then the mesoporous TiO_2 layer composed of 20 nm-sized particles was deposited by spin coating at 5000 rpm for 30 s using a commercial TiO_2 paste (Dyesol 18NRT, Dyesol) diluted in ethanol with different ratios. After drying at 125 °C, the TiO_2 films were gradually heated to 500 °C, baked at this temperature for 15 min and cooled to room temperature. The thickness of mp-TiO_2 film was measured by a Profile-system (DEKTAK 150, VECCO, Bruker). Prior to their use, the films were again dried at 500 °C for 30 min. PbI_2 was dissolved in *N*,*N*-dimethylformamide at a concentration of 510 mg mL^{-1} under stirring at 70 °C. The solution was kept at 70 °C during the whole device fabrication procedure. The mesoporous TiO_2 films were then infiltrated with PbI_2 by spin coating at 6500 rpm for 90 s and dried at 70 °C for 30 min. After cooling to room temperature, the films were dipped in a solution of CH_3NH_3I in 2-propanol (8 mg mL^{-1}) for 30 s, rinsed with 2-propanol and dried at 70 °C for 30 min. The HTM was then deposited by spin coating at 4000 rpm for 30 s. The spin-coating formulation was prepared by dissolving 72.3 mg spiro-MeOTAD, 28.8 μL 4-*tert*-butylpyridine, 17.5 μL of a stock solution of 520 mg mL^{-1} LiTFSI lithium bis-(trifluoromethyl- sulphonyl)imide in acetonitrile. Finally, gold was thermally evaporated on top of the device to form the back contact. The device fabrication was carried out in the glovebox with a dry air atmosphere and the humidity of water <20 ppm.

Supercapacitor Device Fabrication. Bacterial cellulose (BC) membrane was prepared and purified according to the method previously. The synthetic route for BC nanofibers suspension was similar to that which has been previously reported,[34,35] then the nanofibers suspension was diluted into 2 mg mL^{-1}. A volume of 35 mL of BC nanofibers suspension was added into 35 mL hydrochloric acid (2.0 M) with 10 mM ferric chloride solution followed by 20 min of sonication, and then 0.35 mL pyrrole monomer was added into the mixture under stirring when the temperature cooled to 4 °C in an ice bath. After that, the mixture was stirred in the ice bath for another 2 h. The obtained black composites were collected using a vacuum filtration method after being washed several times with deionized water, and then the nanofibers were redispersed into deionized water by using a hand blender. Suspensions of BC/PPy nanofibers and a certain amount of modified MWCNTs were sonicated using sodium dodecyl benzenesulfonate (SDBS) as surfactant for 30 min to ensure the sufficient mixing. The as-obtained suspension was kept at rest for 3 h to make sure the MWCNTs assembled with BC/PPy nanofibers, then the suspension was vacuum filtrated to form a filter cake, which was subsequently washed several times with 0.3 M hydrochloric acid and deionized water. The washed filter cake was then dried at 70 °C for 12 h and peeled off to get a freestanding membrane. The symmetric supercapacitor tests were conducted in a 2032-type cell with two BC/PPy nanofibers/MWCNTs films (with a size of around 1 cm × 1 cm) as electrodes and a cellulose acetate membrane as a separator.

Photovoltaic Characterization. A 450 W xenon light source solar simulator (Oriel, model 9119) with AM 1.5G filter (Oriel, model 91192) was used to give an irradiance of 100 mW cm^{-2} at the surface of the solar cell. The current−voltage characteristics of the cell under these conditions were obtained by applying external potential biases to the cell and measuring the generated photocurrents with a Keithley model 2400 digital source meter. A similar data acquisition system was used to control the IPCE measurement. A white light bias (1% sunlight intensity) was applied onto the sample during the IPCE measurements with ac model (10 Hz).

Transient Photovoltage/Photocurrent Decay Measurement. For the transient decay measurement, a white light bias on the device sample was generated from an array of diodes. Blue light pulse diodes (0.05 s square pulse width, 100 ns rise and fall time) controlled by a fast solid-state switch were used as the perturbation source. The voltage/current dynamics were recorded on a PC-interfaced Keithley 2602A source meter with a 100 μs response time. The transient photovoltage or photocurrent decay responding to the perturbation signal was performed where a bias of voltage or current was applied onto the device. The bias (voltage or current) is provided by the Keithley 2602A, which compensates to the open circuit voltage or the short circuit current of the device responded to the white LED. In this case, the lifetime and diffusion coefficient can be extracted at the same condition. The perturbation light source was set to a suitably low level in order for the voltage decay kinetics to be monoexponential. By varying the white light bias intensity, we could estimate the recombination lifetime over a wide range. Before the LEDs switched to the next light intensity, a charge extraction routine was executed to measure the electron density in the film. In the charge extraction techniques, the LED illumination source was turned off in <300 ns, while simultaneously, the cell was switched from open to short circuit (in about 200 ns). The resulting current, as the cell returns to $V = 0$ and $J = 0$, was integrated to give a direct measurement of the excess charge in the film at that V_{OC}.

Conflict of Interest: The authors declare no competing financial interest.

Supporting Information Available: SEM image for samples. This material is available free of charge *via* the Internet at http://pubs.acs.org.

Acknowledgment. Financial support from the 973 Program of China (2014CB643506, 2013CB922104, and 2011CBA00703), NSFC (21103057, 21161160445, and 21173091), the Innovation Fund of Innovation Institute (HUST, CXY13Q009) and the CME with the Program of New Century Excellent Talents in University

(NCET-10-0416), is gratefully acknowledged. The authors thank the Analytical and Testing Centre at the HUST for performing the characterization of various samples.

REFERENCES AND NOTES

1. Fan, X.; Zhang, M.; Wang, X.; Yang, F.; Meng, X. Recent Progress in Organic–Inorganic Hybrid Solar Cells. *J. Mater. Chem. A* **2013**, *1*, 8694–8709.
2. Liang, P.; Liao, C.; Chueh, C.; Zuo, F.; Williams, S.; Xin, X.; Lin, J.; Jen, A. Additive Enhanced Crystallization of Solution-Processed Perovskite for Highly Efficient Planar-Heterojunction Solar Cells. *Adv. Mater.* **2014**, *26*, 3748–3754.
3. Kim, H.-S.; Lee, C.-R.; Im, J.-H.; Lee, K.-B.; Moehl, T.; Marchioro, A.; Moon, S.-J.; Humphry-Baker, R.; Yum, J.-H.; Moser, J. E.; et al. Lead Iodide Perovskite Sensitized All-Solid-State Submicron Thin Film Mesoscopic Solar Cell with Efficiency Exceeding 9%. *Sci. Rep.* **2012**, *2*, 591.
4. Wehrenfennig, C.; Eperon, G.; Johnston, M.; Snaith, H.; Herz, L. High Charge Carrier Mobilities and Lifetimes in Organolead Trihalide Perovskites. *Adv. Mater.* **2013**, *26*, 1584–1589.
5. Xiao, Z.; Bi, C.; Shao, Y.; Dong, Q.; Wang, Q.; Yuan, Y.; Wang, C.; Gao, Y.; Huang, J. Efficient, High Yield Perovskite Photovoltaic Devices Grown by Interdiffusion of Solution-Processed Precursor Stacking Layers. *Energy Environ. Sci.* **2014**, *7*, 2619.
6. Lee, M.; Teuscher, J.; Miyasaka, T.; Murakami, T.; Snaith, H. Efficient Hybrid Solar Cells Based on Meso-Superstructured Organometal Halide Perovskites. *Science* **2012**, *338*, 643–647.
7. Etgar, L.; Gao, P.; Xue, Z.; Peng, Q.; Chandiran, A.; Liu, B.; Nazeeruddin, M.; Grätzel, M. Mesoscopic $CH_3NH_3PbI_3/TiO_2$ Heterojunction Solar Cells. *J. Am. Chem. Soc.* **2012**, *134*, 17396–17399.
8. Xing, G.; Mathews, N.; Sun, S.; Lim, S.; Lam, Y.; Grätzel, M.; Mhaisalkar, S.; Sum, T. Long-Range Balanced Electron- and Hole-Transport Lengths in Organic-Inorganic $CH_3NH_3PbI_3$. *Science* **2013**, *342*, 344–347.
9. Stranks, S.; Eperon, G.; Grancini, G.; Menelaou, C.; Alcocer, M.; Leijtens, T.; Herz, L.; Petrozza, A.; Snaith, H. Electron-Hole Diffusion Lengths Exceeding 1 Micrometer in an Organometal Trihalide Perovskite Absorber. *Science* **2013**, *342*, 341–344.
10. Burschka, J.; Pellet, N.; Moon, S.; Humphry-Baker, R.; Gao, P.; Nazeeruddin, M.; Grätzel, M. Sequential Deposition as A Route to High-Performance Perovskite-Sensitized Solar Cells. *Nature* **2013**, *499*, 316.
11. Liu, M.; Johnston, M.; Snaith, H. Efficient Planar Heterojunction Perovskite Solar Cells by Vapour Deposition. *Nature* **2013**, *501*, 395.
12. Jeon, N.; Lee, F.; Kim, Y.; Seo, J.; Noh, J.; Lee, J.; Seok, S. *o*-Methoxy Substituents in Spiro-OMeTAD for Efficient Inorganic–Organic Hybrid Perovskite Solar Cells. *J. Am. Chem. Soc.* **2014**, *136*, 7837–7840.
13. Im, J.-H.; Jang, I.-H.; Pellet, N.; Grätzel, M.; Park, N.-G. Growth of $CH_3NH_3PbI_3$ Cuboids with Controlled Size for High-Efficiency Perovskite Solar Cells. *Nat. Nanotechnol.* **2014**, *9*, 927–932.
14. Zhou, H.; Chen, Q.; Li, G.; Luo, S.; Song, T.; Duan, H.; Hong, Z.; You, J.; Liu, Y.; Yang, Y. Interface Engineering of Highly Efficient Perovskite Solar Cells. *Science* **2014**, *345*, 542–546.
15. Snaith, H. Perovskites: The Emergence of a New Era for Low-Cost, High-Efficiency Solar Cells. *J. Phys. Chem. Lett.* **2013**, *4*, 3623–3630.
16. Unger, E.; Hoke, E.; Bailie, C.; Nguyen, W.; Bowring, A.; Heumüller, T.; Christoforo, M.; McGehee, M. Hysteresis and Transient Behavior in Current–Voltage Measurements of Hybrid-Perovskite Absorber Solar Cells. *Energy Environ. Sci.* **2014**, *7*, 3690–3698.
17. Tian, Y.; Cong, S.; Su, W.; Chen, H.; Li, Q.; Geng, F.; Zhao, Z. Synergy of W18O49 and Polyaniline for Smart Supercapacitor Electrode Integrated with Energy Level Indicating Functionality. *Nano Lett.* **2014**, *14*, 2150–2156.
18. Guo, W.; Xue, X.; Wang, S.; Lin, C.; Wang, Z. An Integrated Power Pack of Dye-Sensitized Solar Cell and Li Battery Based on Double-Sided TiO_2 Nanotube Arrays. *Nano Lett.* **2012**, *12*, 2520–2523.
19. Bae, J.; Park, Y.; Lee, M.; Cha, S.; Chi, Y.; Lee, C.; Kim, J.; Wang, Z. Single-Fiber-Based Hybridization of Energy Converters and Storage Units Using Graphene as Electrodes. *Adv. Mater.* **2011**, *23*, 3446–3449.
20. Chen, T.; Qiu, L.; Yang, Z.; Cai, Z.; Ren, J.; Li, H.; Lin, H.; Sun, X.; Peng, H. An Integrated "Energy Wire" for both Photoelectric Conversion and Energy Storage. *Angew. Chem., Int. Ed.* **2012**, *51*, 11977–11980.
21. Chen, X.; Sun, H.; Yang, Z.; Guan, G.; Zhang, Z.; Qiu, L.; Peng, H. A Novel "Energy Fiber" by Coaxially Integrating Dye-Sensitized Solar Cell and Electrochemical Capacitor. *J. Mater. Chem. A* **2014**, *2*, 1897–1902.
22. Wang, X.; Liu, B.; Liu, R.; Wang, Q.; Hou, X.; Chen, D.; Wang, R.; Shen, G. Fiber-Based Flexible All-Solid-State Asymmetric Supercapacitors for Integrated Photodetecting System. *Angew. Chem., Int. Ed.* **2014**, *53*, 1849–1853.
23. Fu, Y.; Wu, H.; Ye, S.; Cai, X.; Yu, X.; Hou, S.; Kafafy, H.; Zou, D. Integrated Power Fiber for Energy Conversion and Storage. *Energy Environ. Sci.* **2013**, *6*, 805–812.
24. Wang, M.; Grätzel, C.; Zakeeruddin, S.; Grätzel, M. Recent Developments in Redox Electrolytes for Dye-Sensitized Solar Cells. *Energy Environ. Sci.* **2012**, *5*, 9394–9405.
25. Sum, T.; Mathews, N. Advancements in Perovskite Solar Cells: Photophysics Behind the Photovoltaics. *Energy Environ. Sci.* **2014**, *7*, 2518–2534.
26. Edri, E.; Kirmayer, S.; Henning, A.; Mukhopadhyay, S.; Gartsman, K.; Rosenwaks, Y.; Hodes, G.; Cahen, D. Why Lead Methylammonium Tri-Iodide Perovskite-Based Solar Cells Require a Mesoporous Electron Transporting Scaffold (but Not Necessarily a Hole Conductor). *Nano Lett.* **2014**, *14*, 1000–1004.
27. Juarez-Perez, E.; Wuβler, M.; Fabregat-Santiago, F.; Lakus-Wollny, K.; Mankel, E.; Mayer, T.; Jaegermann, W.; Mora-Sero, I. Role of the Selective Contacts in the Performance of Lead Halide Perovskite Solar Cells. *J. Phys. Chem. Lett.* **2014**, *5*, 680–685.
28. Zheng, L.; Ma, Y.; Chu, S.; Wang, S.; Qu, B.; Xiao, L.; Chen, Z.; Gong, Q.; Wu, Z.; Hou, X. Improved Light Absorption and Charge Transport for Perovskite Solar Cells with Rough Interfaces by Sequential Deposition. *Nanoscale* **2014**, *6*, 8171–8176.
29. Heo, J.; Im, S.; Noh, J.; Mandal, T.; Lim, C.; Chang, J.; Lee, Y.; Kim, H.; Sarkar, A.; Nazeeruddin, M.; et al. Efficient Inorganic–Organic Hybrid Heterojunction Solar Cells Containing Perovskite Compound and Polymeric Hole Conductors. *Nat. Photonics* **2013**, *7*, 486–491.
30. Boix, P.; Nonomura, K.; Mathews, N.; Mhaisalkar, S. Current Progress and Future Perspectives for Organic/Inorganic Perovskite Solar Cells. *Mater. Today* **2014**, *17*, 16–23.
31. Eperon, G.; Stranks, S.; Menelaou, C.; Johnston, M.; Herz, L.; Snaith, H. Formamidinium Lead Trihalide: A Broadly Tunable Perovskite for Efficient Planar Heterojunction Solar Cells. *Energy Environ. Sci.* **2014**, *7*, 982–988.
32. Pellet, N.; Gao, P.; Gregori, G.; Yang, T.; Nazeeruddin, M.; Maier, J.; Grätzel, M. *Angew. Chem., Int. Ed.* **2014**, *53*, 3151–3157.
33. Xu, X.; Zhang, H.; Cao, K.; Cui, J.; Lu, J.; Zeng, X.; Shen, Y.; Wang, M. Lead Methylammonium Triiodide Perovskite-Based Solar Cells: An Interfacial Charge-Transfer Investigation. *ChemSusChem* **2014**, *7*, 3088–3094.
34. Li, S.; Huang, D.; Zhang, B.; Xu, X.; Wang, M.; Yang, G.; Shen, Y. Flexible Supercapacitors Based on Bacterial Cellulose Paper Electrodes. *Adv. Energy Mater.* **2014**, *4*, DOI: 10.1002/aenm.201301655.
35. Li, S.; Huang, D.; Yang, J.; Zhang, B.; Zhang, X.; Yang, G.; Wang, M.; Shen, Y. Freestanding bacterial cellulose–polypyrrole nanofibres paper electrodes for advanced energy storage devices. *Nano Energy* **2014**, *9*, 309–317.